ACTIVE POWER CONTROL IN PV SYSTEMS USING A CURVE FITTING ALGORITHM BASED ON THE SINGLE-DIODE MODEL

Efstratios BATZELIS[(1)] Theofanis SOFIANOPOULOS[(1)] Stavros PAPATHANASSIOU[(1)]

[(1)] NTUA, Electric Power Division, 9 Iroon Polytechniou str., 15780, Athens, Greece

e-mail: batzelis@mail.ntua.gr, fanis.sofianopoulos@gmail.com, st@power.ece.ntua.gr

ABSTRACT: In order for a PV system to offer ancillary services to the grid, it should be capable of maintaining active power reserves and controlling its output power. In this paper, such a power regulation technique is proposed, which is based on an improved algorithm to estimate the maximum available power when operating suboptimally. The method introduced employs the fundamental equation of the single-diode PV model and applies linear least squares curve fitting to provide the model parameters in an analytical and computationally efficient way. The effectiveness of the control strategy is validated through simulations in MATLAB/Simulink, recording the system's response in irradiance/temperature variations and reserve command step changes, in both noiseless and noisy environment. Results show excellent dynamic response and increased accuracy and reliability compared to previous approaches.
Keywords: Active power control, Curve fitting, Linear least squares, Maximum power, Photovoltaic system, Power reserves, Single diode model.

1 INTRODUCTION

To allow large-scale penetration of photovoltaic (PV) and other intermittent renewable energy sources (RES), network codes demand that the plants provide ancillary services to the grid. These services usually include contribution to frequency regulation, low voltage ride through (LVRT) capability, or even power curtailments e.g. in small isolated electric networks due to penetration limitations. In order for a PV system to offer such services, it should be capable of controlling its output power and maintaining active power reserves in response to commands issued by the grid operator.

In order for a PV plant to offer power regulation capability, either energy storage has to be installed or a control technique has to be employed, enabling operation at a suboptimal operating point, rather than at the maximum power point (MPP). The former approach entails increased cost and system complexity [1], thus several studies propose output power curtailment to maintain power reserves and provide frequency regulation [2]–[5], albeit they do not address PV power control at a given setpoint, in order to maintain specific power reserves.

For this purpose, the maximum available power of the PV system needs to be continuously known, even when the PV system operates far from the MPP. Some model-based MPP tracking methods found in the literature estimate the MPP using past measurements of a few operating points [6]–[8], while others employ a curve fitting procedure to cope with noise in measurements [9]–[11]. However, the above studies rely on iterative determination of the MPP, which is not practical for implementation in a microcontroller, except for [6] that uses a quadratic model, however based on only three measurements, and [10] which needs *a priori* adaptation of the model parameters to the study-case system.

Previous work presented in [12] uses only 2 operating points to estimate the MPP in a hybrid linear-quadratic way, leading to noise susceptibility and estimation errors. This problem is circumvented in [13], by employing a curve fitting technique based on a quadratic model, however accuracy of the maximum power estimation still remains moderate.

This is resolved in this paper, employing the fundamental equation of the single-diode model in the curve fitting procedure for increased accuracy, while the *linear* least squares (LSQ) optimization is still applied. Therefore, the simplicity and explicit form of the equations involved are retained, leading to a robust and computationally efficient method, suitable for implementation in a microcontroller. This paper is practically an improvement of the work presented in [13], while the effectiveness of the proposed method is tested through simulations in MATLAB/Simulink assuming noise in measurements and simultaneous irradiance and temperature variation.

In Section 2 of this paper, the topology of the proposed control scheme is presented, while the MPP estimation algorithm employed is described in detail in Section 3. Simulation results are discussed in Section 4, followed by conclusions in Section 5.

2 POWER CONTROL SCHEME

The proposed topology and control scheme is illustrated in Figure 1. The photovoltaic energy is transferred through a boost converter to the inverter, which in turn feeds in the electric grid, implementing a P-Q control and ancillary services policy. This way, the DC link voltage is kept constant and the converter receives a reserve command r that corresponds to the desired power reserves, expressed as a fraction of the maximum available PV power. Regulation of the PV output is made by adjusting the duty cycle D of the PWM regulator of the DC/DC converter.

The duty cycle is adjusted by a PI controller that regulates the output power P_{pv} to its reference value P_{ref}, determined according to the power reserve command and the maximum available power P_{mp}. It is worth noting that the monotonicity of the power with respect to the duty cycle differs on the two sides of the *P-V* curve (right and left of the MPP), hence the sign of the voltage error is used in Figure 1, to enable operation of the controller over the entire voltage range.

The controller described above requires knowledge of the MPP power and voltage, obtained through the *MPP estimator* block, which employs *linear* LSQ curve fitting on a set of recent past measurements (V_m, I_m) to determine model parameters and then the MPP attributes. Details of this algorithm are discussed in Section 3.

The control scheme will inevitably experience noise in

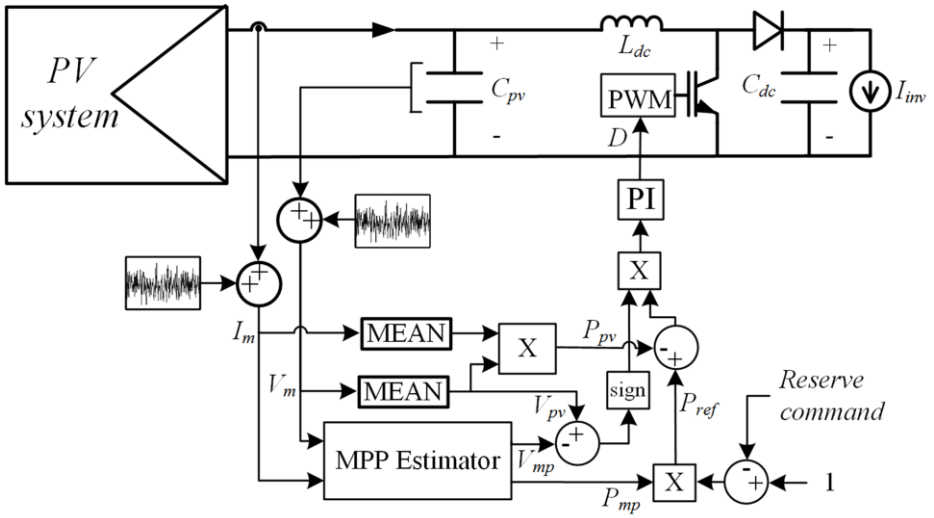

Figure 1: Simplified power circuit and control scheme of the proposed technique.

measurements, due to electromagnetic interference (EMI) from the power circuit, modeled as additive white Gaussian noise (AWGN) superposed on voltage and current measurements in Figure 1. The PV voltage V_{pv} and power P_{pv} utilized in the controller are obtained by averaging over the control period, effectively eliminating noise and switching ripple. It is worth noting that the curve fitting algorithm involved in the MPP estimator is inherently robust in presence of such fluctuations with a zero mean value.

3 MPP ESTIMATOR

The control strategy presented requires knowledge of the MPP voltage and power, even when operating at a suboptimal point, possibly far from the MPP. For this purpose, the fundamental equation of the single-diode PV model is used and a curve fitting algorithm is applied to previous measurements to approximate the model parameters, and therefore the MPP.

If the shunt resistance is ignored, the equivalent circuit of the single-diode model shown in Figure 2 is obtained, where the *I-V* relation is given by (1):

$$I = I_{ph} - I_s e^{(V+IR_s)/a} \tag{1}$$

This equation is fitted to a certain number of past measurements, included in a measurement window, in order to determine the four model parameters I_{ph}, I_s, a and R_s. Thereafter, the MPP voltage, current and power are calculated by the simple explicit expressions proposed in [14]:

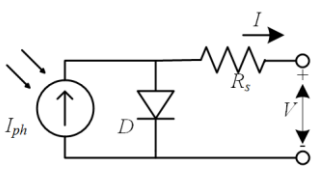

Figure 2: Electrical equivalent circuit of the single-diode model neglecting the shunt resistance. There are four model parameters: I_{ph}, I_s, a and R_s.

$$V_{mp} = a(w-1) - R_s I_{ph}(1-1/w) \tag{2}$$

$$I_{mp} = I_{ph}(1-1/w) \tag{3}$$

$$P_{mp} = V_{mp} I_{mp} \tag{4}$$

where $w=W\{I_{ph}e/I_s\}$ and $W\{x\}$ corresponds to the Lambert *W* function. The latter is supported in MATLAB, but in this paper the series expansion proposed in [15] is adopted for more efficient computation.

It is worth noting that neglecting the shunt resistance R_{sh} does not considerably affect the accuracy of the model, due to operation at the right-hand side of the *P-V* curve, where the effect of R_{sh} is quite limited.

To facilitate understanding, an indicative scenario is illustrated in Figure 3. Given a measurement window of *n* past measurements (V_i, P_i) (green dots) around the current operating point, the least squares method minimizes the sum of squared ordinal deviations between estimated and measured values, by zeroing the partial derivatives with respect to each parameter [16]. This way the model parameters are determined, the *P-V* curve may be extrapolated (red line) and the MPP is calculated using (2) -(4) (red circle marker).

In order to apply *linear* LSQ curve fitting and derive simple analytical expressions for the model parameters, as in [13], the four parameters must be linearly independent. However, this is not the case for the fundamental equation of the model, due to its exponential term. To overcome this

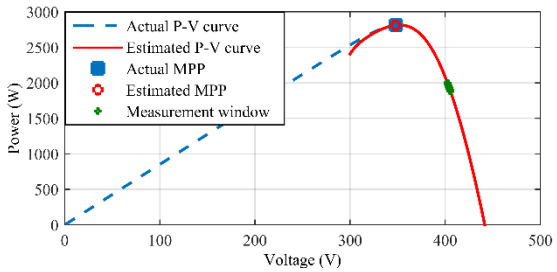

Figure 3: Indicative scenario of MPP estimation maintaining a power reserve of 30%. Given a set of past measurements (green dots), the model parameters are calculated through *linear* LSQ curve fitting and the MPP is then estimated (red circle).

issue, the four parameters are calculated in two stages: first a and R_s are extrapolated to actual temperature using extrapolation equations, and then I_{ph} and I_s are determined using *linear* LSQ minimization.

3.1 Extrapolation of a and R_s to actual temperature

Most studies in literature that adopt the single-diode PV model, consider proportional dependency of the modified diode ideality factor a on the temperature and no irradiance effect [17]. Furthermore, usually the series resistance is assumed almost constant and independent on the operating conditions. Thus, the actual values of a and R_s are calculated by:

$$a = a_0 \frac{T_c}{T_0} \qquad R_s = R_{s0} \tag{5}$$

where a_0 and R_{s0} refer to the STC values of the two parameters, while T_c and T_0 to the actual and nominal temperatures (in Kelvin degrees).

Although a_0 and R_{s0} may be derived offline and provided as inputs to the algorithm, this probably leads to inaccuracies, since the actual characteristics of the PV array may differ from the modules datasheet values, while they are modified over the years due to ageing. To cope with this, a *parameter identification* procedure is assumed to take place periodically on an infrequent basis (e.g. once per month or year), to correctly determine all parameters of the model. This process involves scanning of the entire *P-V* characteristic, followed by application of conventional iterative *non-linear* LSQ curve fitting. The values of a and R_s thus calculated are extrapolated back to nominal temperature T_0 and the updated reference parameters a_0 and R_{s0} are acquired. A temperature sensor required in this procedure is always included in the monitoring equipment of the PV system.

3.2 Calculation of I_{ph} and I_s via *linear* LSQ curve fitting

Given the known values of a and R_s from the previous stage, the *linear* LSQ theorem states that I_{ph} and I_s are given by [9]:

$$\begin{bmatrix} 1 & 1 & \dots & 1 \\ e^{\frac{V_1+I_1R_s}{a}} & e^{\frac{V_2+I_2R_s}{a}} & \dots & e^{\frac{V_n+I_nR_s}{a}} \end{bmatrix} \begin{bmatrix} 1 & e^{\frac{V_1+I_1R_s}{a}} \\ 1 & e^{\frac{V_2+I_2R_s}{a}} \\ \vdots & \vdots \\ 1 & e^{\frac{V_n+I_nR_s}{a}} \end{bmatrix} \begin{bmatrix} I_{ph} \\ I_s \end{bmatrix} = \begin{bmatrix} 1 & 1 & \dots & 1 \\ e^{\frac{V_1+I_1R_s}{a}} & e^{\frac{V_2+I_2R_s}{a}} & \dots & e^{\frac{V_n+I_nR_s}{a}} \end{bmatrix} \begin{bmatrix} I_1 \\ I_2 \\ \vdots \\ I_n \end{bmatrix} \tag{6}$$

Multiplication of the matrices leads to the linear two equation system (7):

$$\begin{bmatrix} S_{00} & -S_{01} \\ S_{01} & -S_{02} \end{bmatrix} \begin{bmatrix} I_{ph} \\ I_s \end{bmatrix} = \begin{bmatrix} S_{10} \\ S_{11} \end{bmatrix} \tag{7}$$

where the notation $S_{xy} = \sum_{i=1}^{n} I_i^x e^{y(V_i+I_iR_s)/a}$ is used. If this linear system is symbolically solved, the following analytical expressions are derived for I_{ph} and I_s:

$$I_{ph} = \frac{S_{10}S_{02} - S_{01}S_{11}}{S_{00}S_{02} - S_{01}^2}, \quad I_s = \frac{S_{00}I_{ph} - S_{10}}{S_{01}} \tag{8}$$

Consequently, the final two parameters are estimated through the simple equations (8) in a straightforward manner, without any need for iterative procedures.

The calculation of sums S_{xy} needed in (8) is made recursively for reduced computational burden. Specifically, at each step k the value of the sum is updated with the latest measurement, while the oldest measurement is removed from the window, leading to minimum computational cost:

$$S_{xy}^k = \sum_{i=k}^{k+n} I_i^x e^{y(V_i+I_iR_s)/a} = S_{xy}^{k-1} + I_{k+n}^x e^{y(V_{k+n}+I_{k+n}R_s)/a} - I_{k-1}^x e^{y(V_{k-1}+I_{k-1}R_s)/a} \tag{9}$$

4 SIMULATION RESULTS

A series of simulations are performed in MATLAB/Simulink to validate the effectiveness and robustness of the control strategy introduced in this paper. The block diagram shown in Figure 1 is built in Simulink, having a boost converter connected to a 2.8 kW PV string (input) and an ideal voltage source at the output, modeling the constant DC link voltage. The characteristics of the PV system are given in Table I.

The system is simulated in simultaneous irradiance/temperature variations and reserve command changes, while two different scenarios are considered: the noiseless case and a low measurement noise case (80 SNR). All simulations are performed using three different window lengths: 10, 100 and 2000 samples.

4.1 Noiseless scenario

The results from the noiseless case are depicted in Figure 4. Trapezoidal irradiance and temperature variations are considered in Figure 4(a), with a high rate of change (40 W/(m^{2}s) and 0.1 °C/s respectively). The reserve command changes are shown in Figure 4(b), varying in the range of 0% to 40%. It is worth noting that the simulation scenario of reserve command and environmental condition changes is a fictitious scenario, only selected as a most severe test of the proposed control algorithm.

Table I: Characteristics of the simulated PV system

Parameter	Value
Nominal PV power	2.8 kW
Input capacitance C_{pv}	470 μF
Inductance L_{dc}	2 mH
DC link voltage	700 V
Switching frequency	10 kHz
Control frequency	83.333 Hz
Sampling frequency	25 kHz
Window length	10, 100, 2000 samples
Noise power	∞ or 80 SNR

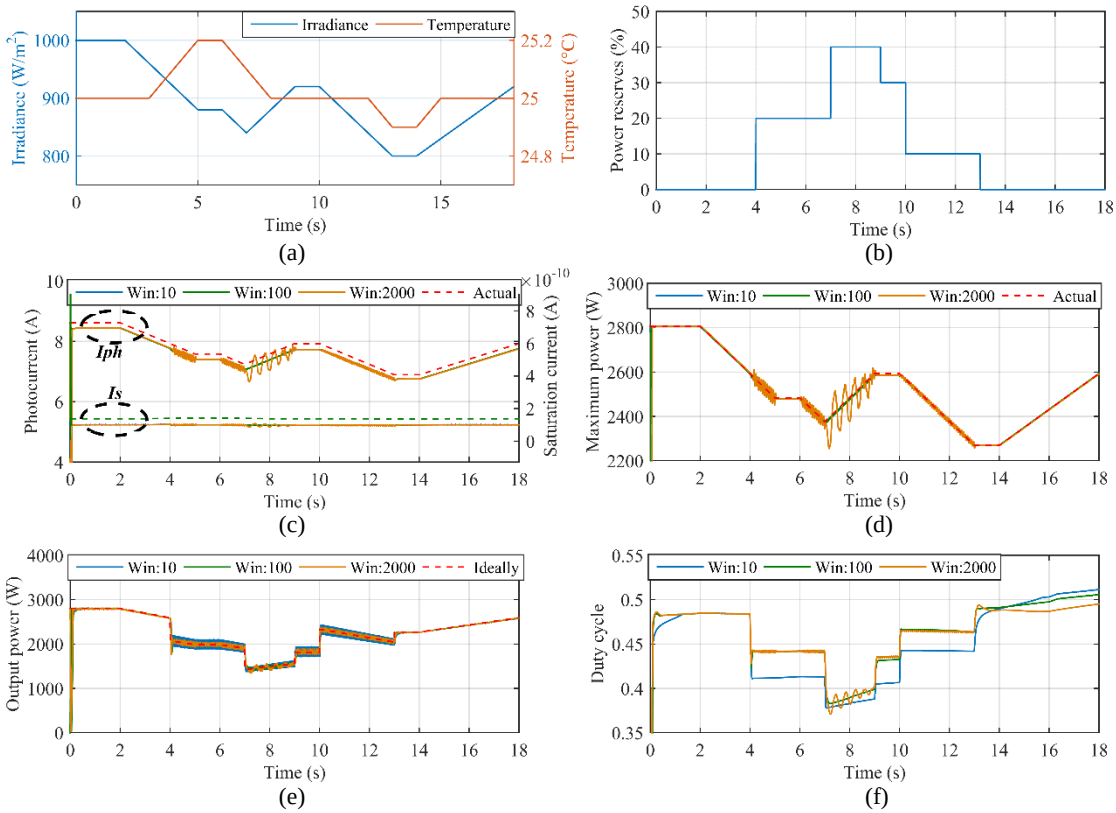

Figure 4: Simulation results of system response in **noiseless** environment, using three different window lengths. (a) Simultaneous irradiance and temperature variations, (b) reserve command step changes, (c) estimated and actual values of model parameters I_{ph} and I_s, (d) estimated and actual maximum available power, (e) actual and requested output power, and (f) duty cycle.

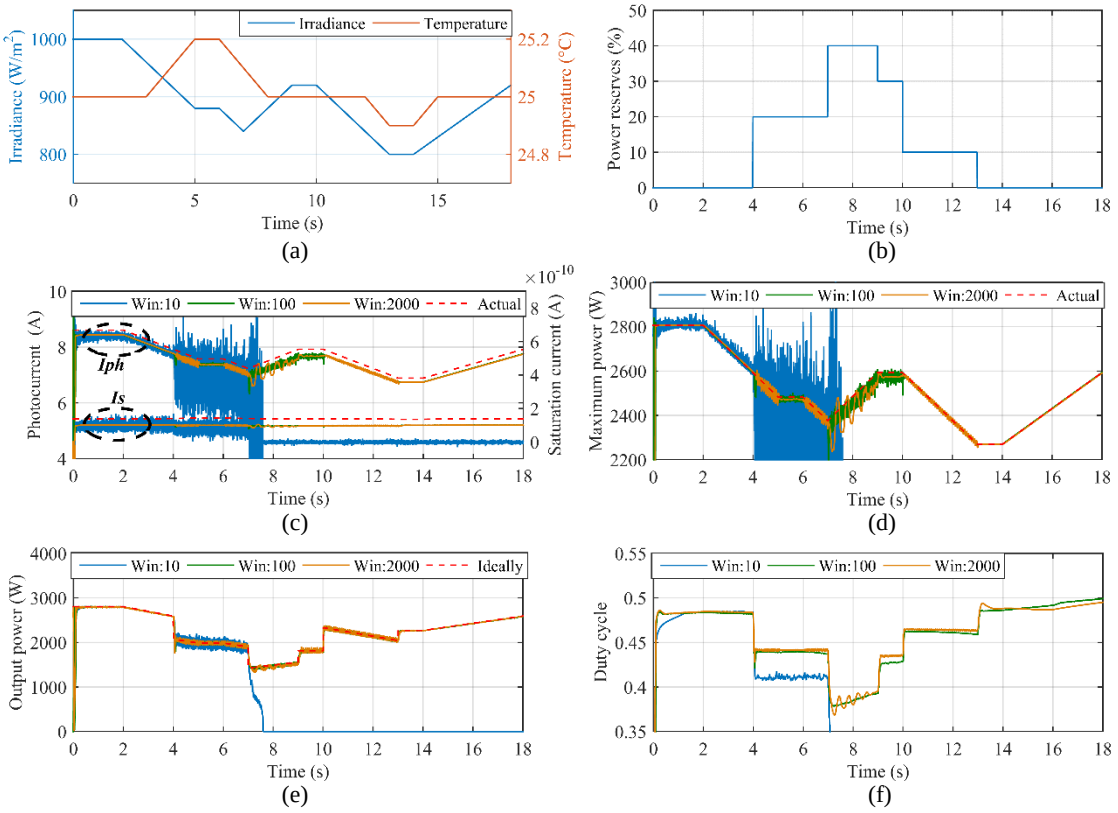

Figure 5: Simulation results of system response in **noisy** environment (SNR 80), using three different window lengths. (a) Simultaneous irradiance and temperature variations, (b) reserve command step changes, (c) estimated and actual values of model parameters I_{ph} and I_s, (d) estimated and actual maximum available power, (e) actual and requested output power, and (f) duty cycle.

The estimated values of model parameters I_{ph} and I_s are depicted in Figure 4(c) for window lengths of 10 (blue line), 100 (green line) and 2000 (orange line) samples and contrasted with their actual values (red dashed lines). Estimates derived with the small (10 samples) and medium (100 samples) window lengths coincide and deviate only slightly from the actual values. The small offset observed is attributed to the model employed (four parameter, rather than the more accurate five parameter one), which necessitates a minor adjustment of the parameters to achieve best fit to the measurements. Nevertheless, the estimated maximum available power proves perfectly accurate over the entire range of the simulation (Figure 4(d)). This is an important observation, which verifies the appropriateness of the model adopted, as well as its independence on the power reserves levels, in contrast to previous works [12]-[13] where the reserve command value affected the accuracy of the estimations.

Using a large window (2000 sample – orange line), on the other hand, leads to erroneous estimates in certain time periods. In particular, at intervals 4-5 s, 6-7 s, and 10-13 s, the estimation presents ripple. A marked fluctuation becomes evident between 7-9 s (Figure 4(c)), when the environmental conditions (mainly the irradiance) change rapidly and the system operates at a suboptimal point maintaining power reserves. This ripple is transferred to the maximum power estimation, as well (Figure 4(d)).

When the window length is too large, measurements recorded may correspond to several instances of a changing *P-V* curve, thus leading to erroneously mixed samples and inaccurate curve fits. It is worth noting that the undesired fluctuation appears from 4 s to 13 s, when operation far from the MPP takes place (Figure 4(b)), but not in the time intervals 5-6 s and 9-10 s, when the irradiance and temperature remain constant (Figure 4(a)). Further, the intensity of the fluctuation is significantly affected by the level of power reserves maintained. This is why the ripple is imperceptible at the time interval 10-13 s, when the reserve command in only 10%, slightly higher at 4-5 s and 6-7 s, when 20% power reserves are required, and even higher during the 7-9 s interval, when the reserve command is the highest. Hence, the curve fitting performance deteriorates when the window length is very large, the operating conditions change rapidly and the operating point is far from the MPP. Similar results regarding the effect of the window length are derived in [13].

The above observations apply to Figure 4(e) as well, where the output power of the PV generator for the three window lengths is compared to the ideal performance. All waveforms are smooth and stable, verifying the effectiveness of the proposed control scheme, with the exception of the large window length in the 7-9 s interval, for the reasons already discussed. Similar conclusions are drawn from Figure 4(f), which shows the PWM duty cycle for the three window alternatives.

4.2 Noisy scenario

The effect of the noise is shown in Figure 5, for the same simulation scenario, assuming AWGN noise in all measurements. In Figure 5(c), where the model parameter estimation is depicted, the small window length now proves unacceptable, as the very few noisy measurements (only 10 samples) are insufficient to accurately model the *P-V* curve. The fluctuation in the parameter estimates becomes very high at 4 s and thereafter, leading to control instability.

On the other hand, the medium window length proves quite satisfactory, presenting accurate model parameter (Figure 5(c)) and maximum power (Figure 5(d)) estimations. A small ripple is evident at the most challenging time intervals, but the system response remains acceptable throughout the entire simulation period.

This is further confirmed with the large window, which presents estimations with even lower high-frequency ripple due to noise (Figure 5(c)-(d)). However, this case suffers during rapid environmental condition variations that cause low-frequency fluctuations as already discussed. It is worth noting that the waveforms of both the model parameters and the maximum power estimates almost coincide between the noiseless and noisy cases, which signifies that, using this window length (2000 samples), the noise has effectively been removed from the measurements. Therefore, the length of the window is an important parameter that should be properly optimized to sufficiently limit the effect of noise and simultaneously permit adaptation to rapid irradiance changes. The same conclusion is reached in [13].

Similar results are extracted from Figure 5(e) and Figure 5(f). The small window leads to control instability shortly before the 8th s, while the medium and large windows lead to quite sufficient performance (except for the 7-9 s interval for the 2000 samples case).

5 CONCLUSION

In this paper, an improved power regulation technique is introduced for a PV system in order to maintain active power reserves. A key point of such a control strategy is the estimation of the maximum available power, when operating far from the MPP. In this study, this is made by employing the fundamental equation of the single-diode PV model and applying *linear* LSQ curve fitting in measurements. The estimation algorithm presents good accuracy and the equations involved are simple and analytical, unlike other implementations which adopt simplified models at the cost of reduced accuracy or employ iterative and computationally inefficient algorithms.

The proposed control strategy is validated through simulations in MATLAB/Simulink assuming reserve command changes, under rapid irradiance and temperature variations. The investigation has shown that the control scheme presents inherent robustness against noise, due to the curve fitting involved, as well as satisfactory tracking performance during rapidly changing environmental conditions. A critical parameter for proper functioning of the controller is the measurement window length, which should be optimized between noise immunity and adaptation to irradiance variations.

6 ACKNOWLEDGMENTS

Mr. E. Batzelis is supported in his PhD studies by "IKY Fellowships of Excellence for Postgraduate Studies in Greece - Siemens Program".

7 REFERENCES

[1] A. Hoke and D. Maksimovic, “Active power control of photovoltaic power systems,” in *Proc.*

2013 1st IEEE Conf. Technol. Sustain. (SusTech 2013), Portland, OR, US, Aug. 2013, pp. 70–77.

[2] V. A. K. Pappu, B. Chowdhury, and R. Bhatt, "Implementing frequency regulation capability in a solar photovoltaic power plant," in *Proc. North Am. Power Symp. 2010 (NAPS 2010)*, Arlington, TX, US, Sep. 2010.

[3] H. Xin, Y. Liu, Z. Wang, D. Gan, and T. Yang, "A new frequency regulation strategy for photovoltaic systems without energy storage," *IEEE Trans. Sustain. Energy*, vol. 4, no. 4, pp. 985–993, Oct. 2013.

[4] A. F. Okou, O. Akhrif, R. Beguenane, and M. Tarbouchi, "Nonlinear control strategy insuring contribution of PV generator to voltage and frequency regulation," in *Proc. 6th IET Int. Conf. Power Electron. Mach. Drives (PEMD 2012)*, Bristol, UK, Mar. 2012, vol. 2012, no. 592 CP, pp. D42–D42.

[5] R. G. Wandhare and V. Agarwal, "Novel control scheme for high power centralized PV-grid system to realize functionalities of AVR and governor as in conventional generators," in *Proc. 37th IEEE Photovolt. Spec. Conf. (PVSC 2011)*, Seattle, WA, US, Jun. 2011, pp. 002460–002465.

[6] F.-S. Pai, R.-M. Chao, S. H. Ko, and T.-S. Lee, "Performance evaluation of parabolic prediction to maximum power point tracking for PV Array," *IEEE Trans. Sustain. Energy*, vol. 2, no. 1, pp. 60–68, Jan. 2010.

[7] J. M. Blanes, F. J. Toledo, S. Montero, and A. Garrigós, "In-site real-time photovoltaic I–V curves and maximum power point estimator," *IEEE Trans. Power Electron.*, vol. 28, no. 3, pp. 1234–1240, Mar. 2013.

[8] A. Garrigós, J. M. Blanes, J. A. Carrasco, and J. B. Ejea, "Real time estimation of photovoltaic modules characteristics and its application to maximum power point operation," *Renew. Energy*, vol. 32, no. 6, pp. 1059–1076, May 2007.

[9] W. Xiao, M. G. J. Lind, W. G. Dunford, and A. Capel, "Real-time identification of optimal operating points in photovoltaic power systems," *IEEE Trans. Ind. Electron.*, vol. 53, no. 4, pp. 1017–1026, Jun. 2006.

[10] A. W. Leedy and K. E. Garcia, "Approximation of P-V characteristic curves for use in maximum power point tracking algorithms," in *Proc. 45th Southeast. Symp. Syst. Theory (SSST 2013)*, Waco, TX, US, Mar. 2013, pp. 88–93.

[11] R. Pradhan and B. Subudhi, "Design and real-time implementation of a new auto-tuned adaptive MPPT control for a photovoltaic system," *Int. J. Electr. Power Energy Syst.*, vol. 64, pp. 792–803, Jan. 2015.

[12] S. Nanou, A. Papakonstantinou, and S. Papathanassiou, "Control of a PV generator to maintain active power reserves during operation," in *Proc. 27th Eur. Photovolt. Sol. Energy Conf. Exhib. (EU PVSEC 2012)*, Frankfurt, Germany, Sep. 2012, pp. 4059–4063.

[13] E. Batzelis, S. Nanou, and S. Papathanassiou, "Active power control in PV systems based on a quadratic curve fitting algorithm for the MPP estimation," in *Proc. 29th Eur. Photovolt. Sol. Energy Conf. Exhib. (EU PVSEC 2014)*, Amsterdam, The Netherlands, Sep. 2014, pp. 3036–3040.

[14] E. I. Batzelis, G. E. Kampitsis, S. A. Papathanassiou, and S. N. Manias, "Direct MPP calculation in terms of the single-diode PV model parameters," *IEEE Trans. Energy Convers.*, vol. 30, no. 1, pp. 226–236, Mar. 2015.

[15] E. I. Batzelis, I. A. Routsolias, and S. A. Papathanassiou, "An explicit PV string model based on the Lambert W function and simplified MPP expressions for operation under partial shading," *IEEE Trans. Sustain. Energy*, vol. 5, no. 1, pp. 301–312, Jan. 2014.

[16] "Least squares." [Online]. Available: http://en.wikipedia.org/wiki/Least_squares.

[17] W. De Soto, S. A. Klein, and W. A. Beckman, "Improvement and validation of a model for photovoltaic array performance," *Sol. Energy*, vol. 80, no. 1, pp. 78–88, Jan. 2006.